PHYSICAL REVIEW MATERIALS **4**, 013403 (2020)

Synthesis and physical properties of the new iridium oxyfluoride $Sr_2Ir(O,F)_{6-\delta}$ using a topochemical reaction method

K. Kuramochi,[1,2,*] T. Shimano,[1,2] T. Nishio,[1] H. Okabe,[3] A. Koda,[3] K. Horigane,[4] J. Akimitsu,[4] and H. Ogino[2,†]
[1]*Department of Physics, Tokyo University of Science, 1–3 Kagurazaka, Shinjuku-ku, Tokyo 162–8601, Japan*
[2]*National Institute of Advanced Industrial Science and Technology (AIST), 1-1-1 Umezono, Tsukuba, Ibaraki 305–8568, Japan*
[3]*Institute of Materials Structure Science/J-PARC Center, High Energy Accelerator Research Organization (KEK), 1-1 Oho, Tsukuba, Ibaraki 305–0801, Japan*
[4]*Research Institute for Interdisciplinary Science, Okayama University, 3-1-1 Tsushima-naka, Kita-ku, Okayama 700–8530, Japan*

(Received 3 October 2019; published 22 January 2020)

We report the synthesis of a new layered iridium oxyfluoride, $Sr_2Ir(O,F)_{6-\delta}$, using a topochemical fluorination method. The c axis is elongated compared to that in the mother compound Sr_2IrO_4, because the fluorine layer is inserted into the rock-salt layer while tetragonal symmetry is preserved. Resistivity measurements for the compound show nonmetallic behavior similar to that of Sr_2IrO_4. In magnetization measurements, suppression of antiferromagnetic order and paramagnetic behavior was observed after topochemical fluorination. Meanwhile, muon spin relaxation (μSR) experiments suggest the development of antiferromagnetic spin correlation between Ir spins. Furthermore, fluorine content was estimated at 1.5 the chemical composition of the fluorinated product being $Sr_2IrO_xF_{1.5}$ with $x = 3.25$, assuming Ir^{4+}. Suppression of magnetic order in $Sr_2Ir(O,F)_{6-\delta}$ is attributed to antiferromagnetic instability between IrO_2 layers by elongation of the c axis due to fluorine intercalation.

DOI: 10.1103/PhysRevMaterials.4.013403

I. INTRODUCTION

The $5d$ transition-metal oxide (TMOs) family has a variety of physical properties arising from large spin-orbit interactions, in contrast to $3d$ TMOs, whose physical properties are strongly affected by the crystal field. Specifically, the Ruddlesden-Popper (RP) type iridate Sr_2IrO_4 has drawn considerable attention due to interesting physical properties such as $J_{\mathrm{eff}} = 1/2$ Mott insulating state induced by a combination of strong spin-orbit interactions and on-site Coulomb repulsion [1,2]. Recently, the possibility of unconventional superconductivity in carrier-doped Sr_2IrO_4 has been proposed because it has several similarities with the high-T_c cuprate superconductors such as La_2CuO_4. It was theoretically suggested that Sr_2IrO_4 exhibits singlet d-wave superconductivity by electron-doping, and triplet p-wave superconductivity by hole-doping [3,4]. Carrier doping such as substitution of La for Sr has already been attempted [5–8], and a metal-insulator transition has been reported in vacancy-introduced Sr_2IrO_4 [9,10]. Moreover, since distinct cuprate phenomena such as a pseudogap-like phase and a d-wave gap have been observed in electron-doped Sr_2IrO_4 [11–13], higher carrier doping may induce bulk superconductivity. Thus, physical properties of new layered compounds containing an IrO_2 plane would be interesting due to their similarity to Sr_2IrO_4.

In recent years, mixed-anion compounds such as oxyhydrides, oxynitrides, and oxyfluorides have attracted attention due to their unique structures and functionalities [14]. By employing a particular low temperature reaction method, namely the topochemical reaction, metastable compounds can be synthesized. Notably, it was reported that topochemical fluorination of RP-type compounds such as $LaSrMnO_4$ and Sr_2TiO_4, yields layered oxyfluorides, $LaSrMnO_4F$ and $Sr_2TiO_3F_2$, respectively [15,16]. These compounds have a TMO_2 plane akin to their mother compounds, while crystallographic anisotropy is enhanced due to fluorine layer insertion into the rock salt layer of their mother compounds. Moreover, physical properties of TMOs are drastically altered by crystal structure modification resulting from topochemical reactions. For instance, it has been reported that $Sr_2CuO_2F_{2+\delta}$ synthesized by topochemical fluorination exhibits superconductivity, in contrast to Mott-insulator nature of its mother compound Sr_2CuO_3 [17]. In addition, $Sr_3Ir_2O_7F_2$, as a layered mixed-anion iridate has recently been synthesized utilizing the topochemical reaction method for RP-type iridate $Sr_3Ir_2O_7$ [18]. It has been reported that physical properties of this material differ from an antiferromagnetic Mott insulating state with half-filled $J_{\mathrm{eff}} = 1/2$ band, to a nonmagnetic $J = 0$ band insulating state, accompanying change in oxidation state from Ir^{4+} to Ir^{5+}. Therefore, applying the topochemical reaction method to Sr_2IrO_4 would be intriguing, in anticipation of a new iridium compound synthesis and the emergence of rich physical properties.

In this study, we attempted to synthesize a new iridium oxyfluoride by topochemical fluorination of Sr_2IrO_4 with various fluorination reagents. Consequently, we successfully synthesized a new layered iridium oxyfluoride $Sr_2Ir(O,F)_{6-\delta}$ by using polyvinylidene difluoride (PVDF), ZnF_2, and CuF_2 as fluorination reagents. Thus, we report its crystal structure and physical properties.

---

[*] kuramochi-kenta@aist.go.jp
[†] h-ogino@aist.go.jp

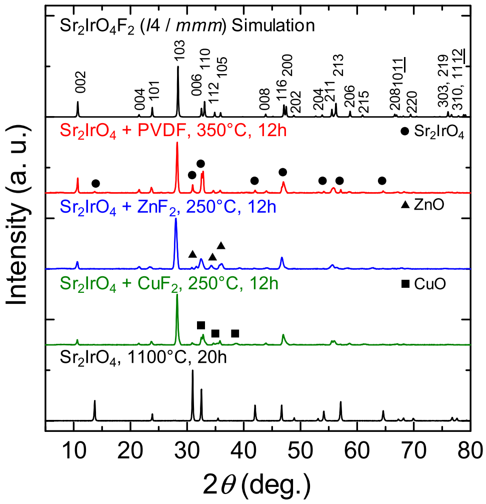

FIG. 1. $Sr_2IrO_4F_2$ simulated XRD pattern and XRD patterns of fluorinated compounds and Sr_2IrO_4.

II. EXPERIMENTAL PROCEDURE

The precursor, Sr_2IrO_4, was synthesized by conventional solid-state reaction methods. Pure metal Ir (3N, Kojundo Chemical Lab. Co., Ltd.) and $SrCO_3$ (4N, Furuuchi Chemical Corporation) were mixed in a 1:2 molar ratio and the mixture sintered in air at 900 °C for 20 h. The powder was reground, mixed into a pellet and again sintered in air at 1100 °C for 20 h.

The precursor was then mixed and pelletized with PVDF (Apollo Scientific Ltd.), ZnF_2 (2N, Kojundo chemical Lab. Co., Ltd.), or CuF_2 (2N, Kojundo chemical Lab. Co., Ltd.) in a 1:1 molar ratio. Samples mixed with PVDF were sintered at 350 °C for 12 h in air, and those mixed with ZnF_2 and CuF_2 were sintered at 250–550 °C for 12 h in air.

Phase identification and calculations of lattice parameters of obtained compounds were interpreted based on powder X-ray diffraction (XRD) data, measured by a Rigaku Ultima-IV at room temperature. The Ir:F ratios of several compounds was measured by a Shimadzu electron probe micro analyzer, EPMA-8050G. Sample resistivities were measured using a four-probe method. Then, samples were pressed at high pressure (3.5 GPa) by cubic-anvil type equipment at room temperature since as-synthesized products were in powder form. Temperature dependence of magnetic susceptibility was carried out by the Quantum-Design magnetic property measurement system, MPMS-XL7, under a magnetic field of 10 kOe. μSR measurements under a zero-field (ZF), and longitudinal fields (LF) were performed using the ARTEMIS spectrometer with a flypast chamber at the Material and Life Science Experimental Facility (MLF), J-PARC, Tokai, Japan [19].

III. RESULTS AND DISCUSSION

A. Crystal structures

Figure 1 shows XRD patterns of precursor, Sr_2IrO_4; samples fluorinated with PVDF, ZnF_2, and CuF_2; and the $Sr_2IrO_4F_2$ simulated pattern. The $Sr_2IrO_4F_2$ hypothetical structure (space group: $I4/mmm$, Supplemental Material [20]) was generated from a minor structure modification of $Ba_2ZrO_3F_2$ (space group: $I4/mmm$) [21]. As the XRD pattern of fluorinated samples corresponded with the $Sr_2IrO_4F_2$ simulation XRD pattern, we surmised that a new layered iridium oxyfluoride $Sr_2Ir(O, F)_{6-\delta}$ was successfully synthesized by topochemical fluorination. Furthermore, all fluorination reagents tested were successful. $Sr_2Ir(O, F)_{6-\delta}$ synthesized by PVDF contained a small amount of unreacted Sr_2IrO_4, and those by TMF_2 (TM = Zn, Cu) contained a small amount of corresponding TMOs as impurities. The schematic figure of Sr_2IrO_4 topochemical fluorination is shown in Fig. 2. Fluorine layer insertion into the rock salt layer consequently elongates the c axis from ~12 Å in Sr_2IrO_4 to 16 Å in $Sr_2Ir(O, F)_{6-\delta}$ as determined by XRD patterns. While observed peaks are in agreement with those of simulated patterns, Rietveld refinement of samples was not possible because of peak broadening and low peak intensity of fluorinated samples. This is probably due to a low crystallinity of products, originating from low reaction temperatures. It has been reported that anion vacancies exist in $Ba_2ZrO_3F_2$, $Ba_2SnO_{2.5}F_3$, and $Sr_2RuO_3F_2$, all of which have a common crystal structure with $Sr_2Ir(O, F)_{6-\delta}$, obtained by fluorination of mono-layered RP type structures [21–23]. Therefore, it is conceivable that anion vacancies are introduced into O/F sites of $Sr_2Ir(O, F)_{6-\delta}$; however, the number of anion vacancies as well as site selectivity of oxygen and fluorine could not be refined. Further studies are needed to establish anion vacancy numbers. Sample lattice parameters subsequent to topochemical reactions at each temperature are plotted in Fig. 3. $Sr_2Ir(O, F)_{6-\delta}$ formation was observed in a temperature range of 250–550 °C. When reaction temperature exceeds 600 °C, other phases such as simple perovskite $SrIrO_3$ and SrF_2 are formed. $Sr_2Ir(O, F)_{6-\delta}$ lattice parameters varied depending on the type of fluorination reagent used and sintering conditions. The variation indicates that there are differences in the O/F ratio and/or anion vacancies in $Sr_2Ir(O, F)_{6-\delta}$, depending on the fluorination conditions. We have performed preliminary compositional analysis on the compounds by EPMA. Average F/Ir ratio of the compounds are 1.20, 1.27, and 1.33 for $Sr_2Ir(O, F)_{6-\delta}$ fluorinated by ZnF_2 at 250, 400, and 550 °C, respectively. However, large fluctuations of the ratio prevent

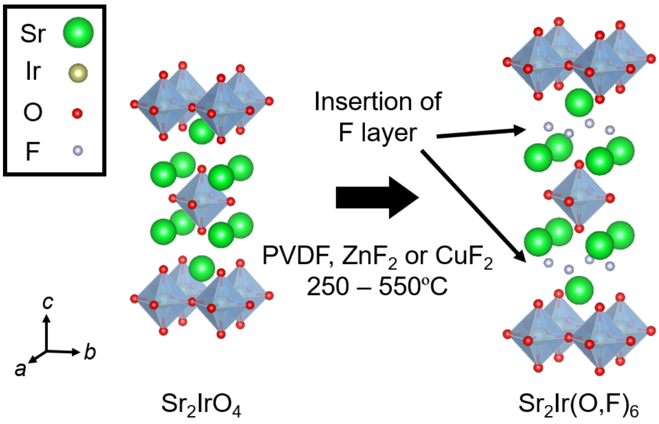

FIG. 2. Schematic of Sr_2IrO_4 topochemical fluorination. Crystal structures are depicted using VESTA [38].

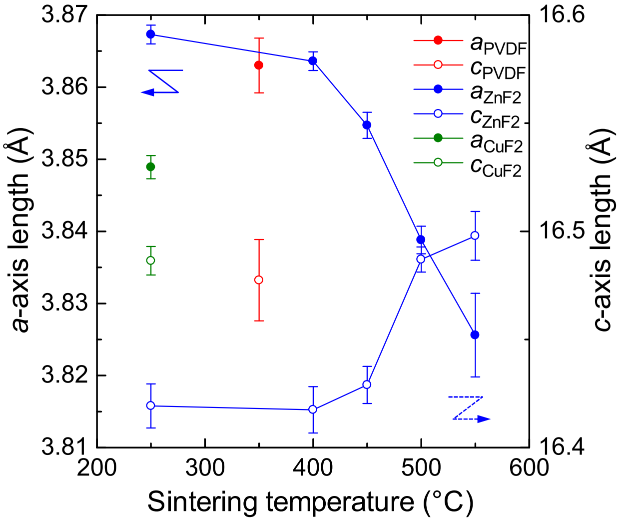

FIG. 3. Fluorination reagents and sintering temperature dependences of lattice parameters.

whether the tendency is intrinsic or not. Further investigations are needed to clarify the point.

B. Resistivity

Figure 4 shows temperature dependence of resistivity for $\mathrm{Sr_2IrO_4}$ and $\mathrm{Sr_2Ir(O,F)_{6-\delta}}$ fluorinated with $\mathrm{ZnF_2}$ at various temperatures. All compounds show nonmetallic behavior without a phase transition from 2 to 300 K. Minor differences in the absolute value of resistivity between the fluorinated compounds are probably due to differences in grain connectivity and variations in $\mathrm{Sr_2Ir(O,F)_{6-\delta}}$ composition resulting from different sintering conditions. The resistivity of these compounds does not obey an Arrhenius law but are well fitted by $[\rho(T) = \rho_0 \exp(T_0/T)^{\nu}]$ with $\nu = 1/2$, which indicates Efros-Shklovskii variable range hopping (VRH) conduction caused by Coulomb interactions between localized electrons [24], as shown in the inset of Fig. 4. The electronic conduction in these systems is not due to simple thermally activated electrons. A similar electronic transport property has been reported in single-crystal $\mathrm{Sr}_{n+1}\mathrm{Ir}_n\mathrm{O}_{3n+1}$ $(n = 1, 2)$ [25,26]. Accordingly, the electronic transport mechanism for the fluorinated compounds seems similar to that observed in layered iridates so far. As the resistivity behavior in the fluorinated phase is similar to that of $\mathrm{Sr_2IrO_4}$, it is considered that a small number of carriers is introduced to $\mathrm{Sr_2IrO_4}$ by topochemical reactions.

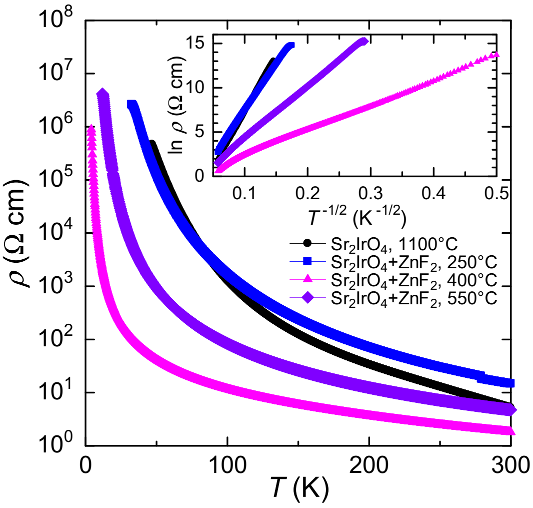

FIG. 4. Resistivity temperature dependence of the mother compound, $\mathrm{Sr_2IrO_4}$, and $\mathrm{Sr_2Ir(O,F)_{6-\delta}}$ fluorinated by $\mathrm{ZnF_2}$. All samples were pressed to pellets at 3.5 GPa at room temperature because as-synthesized samples were obtained in powder form. Inset represents a plot of $\ln(\rho)$ vs. $T^{-1/2}$ for $\mathrm{Sr_2IrO_4}$ and $\mathrm{Sr_2Ir(O,F)_{6-\delta}}$ fluorinated at several temperatures (250, 400, and 550 °C) from 2 to 300 K.

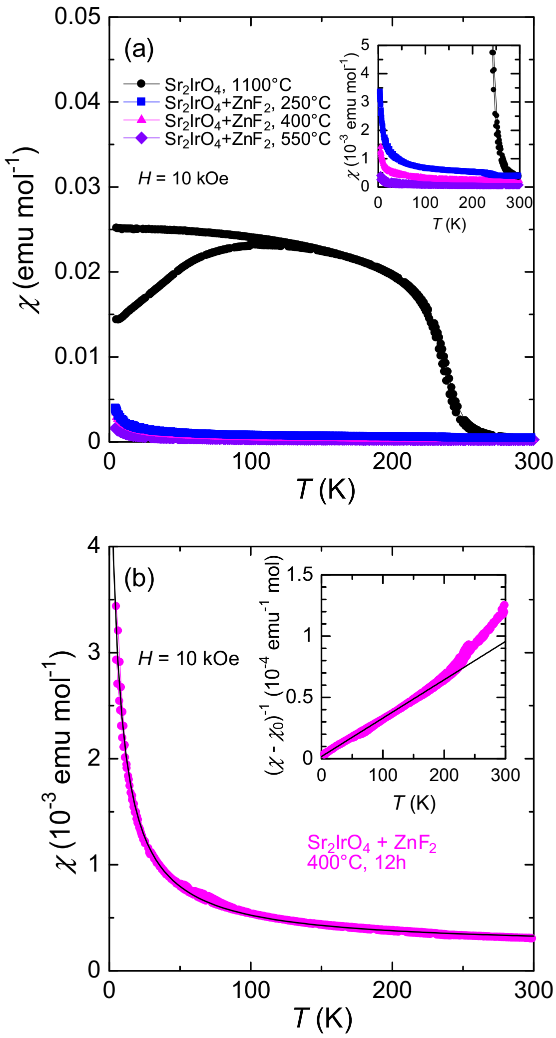

FIG. 5. (a) Magnetic susceptibility temperature dependence of fluorinated samples by $\mathrm{ZnF_2}$ as fluorination reagent measured at 10 kOe. (b) A modified Curie-Weiss fitting for the fluorinated sample with $\mathrm{ZnF_2}$ at 400 °C. Solid line represents the curve-fit.

C. Magnetic susceptibility

Figure 5(a) shows magnetic susceptibility temperature dependence for the mother compound, $\mathrm{Sr_2IrO_4}$, and $\mathrm{Sr_2Ir(O,F)_{6-\delta}}$ fluorinated by $\mathrm{ZnF_2}$ at various temperatures. Following topochemical fluorination, the absolute value of

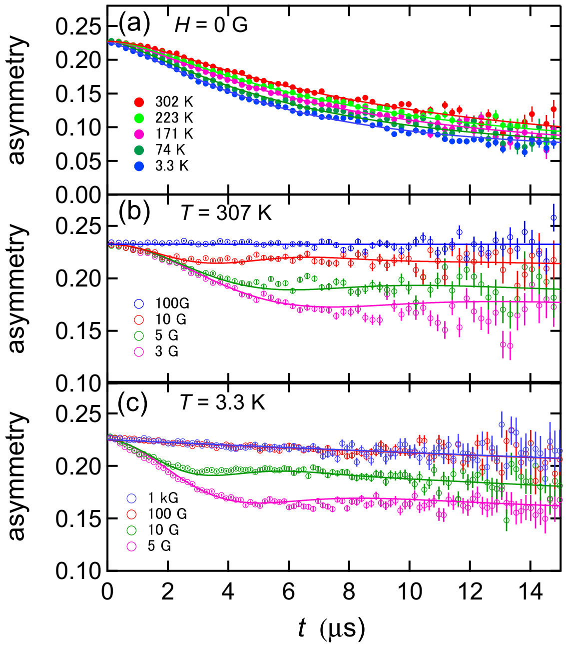

FIG. 6. Typical examples of μSR time spectra in $Sr_2Ir(O, F)_{6-\delta}$ fluorinated with ZnF_2 at 400 °C as representative under (a) zero external field; longitudinal-field μSR time spectra at (b) 307 K and (c) 3.3 K.

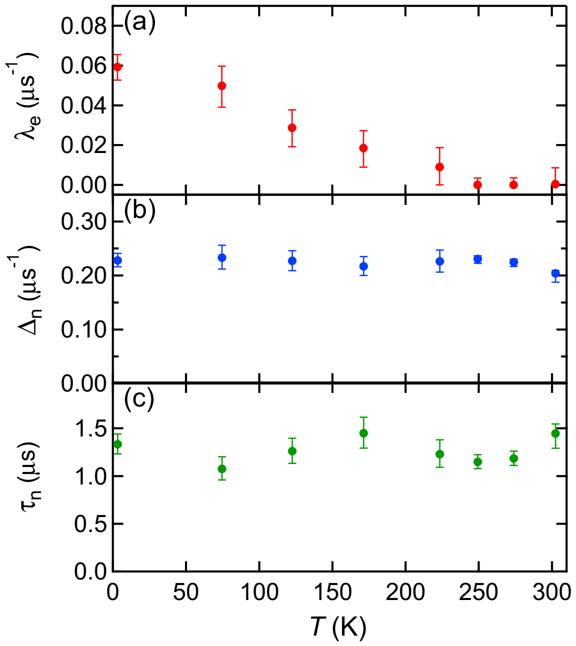

FIG. 7. Temperature dependence of (a) the muon relaxation rate λ_e, (b) the nuclear-field distribution width Δ_n, and (c) correlation time of fluctuation τ_n.

magnetic susceptibility drastically decreases regardless of topochemical conditions. Furthermore, canted antiferromagnetism present in the mother compound Sr_2IrO_4 was not observed in fluorinated compounds, except for the compound synthesized at 250 °C, which is contaminated with a small amount of Sr_2IrO_4. Similar magnetization curves are obtained for $Sr_2Ir(O, F)_{6-\delta}$ fluorinated by CuF_2, except for small contributions from impurities such as Sr_2IrO_4 and CuO (see Fig. S1 in Supplemental Material). As shown in Fig. 5(b), magnetic susceptibility temperature dependence for $Sr_2Ir(O, F)_{6-\delta}$ fluorinated by ZnF_2 was well fitted by a modified Curie-Weiss formula: $\chi(T) = C/(T - \Theta_W) + \chi_0$, where C is the Curie constant, Θ_W is the Weiss temperature, and χ_0 is a small temperature-independent magnetic susceptibility. Parameters obtained from the equation are $C = 3.2 \times 10^{-2}$ emu K mol^{-1}, $\Theta_W = -5.7$ K, and $\chi_0 = 2.2 \times 10^{-4}$ emu mol^{-1} . The effective magnetic moment μ_{eff} calculated from C is 0.51 μ_B. The obtained μ_{eff} is smaller than 1.73 μ_B, which is the local moment expected for Ir^{4+} in the low-spin state, while it is relatively close to 0.40 μ_B, a previously reported value for Sr_2IrO_4 obtained by μSR and neutron diffraction measurements [5,27,28]. It is suggested that $Sr_2Ir(O, F)_{6-\delta}$ magnetism is strongly affected by spin-orbit interactions, unlike that of simple iridium oxides such as Na_2IrO_3 and $Na_4Ir_3O_8$ [29,30].

D. μSR measurements

We performed μSR experiments to investigate the local magnetic state of $Sr_2Ir(O, F)_{6-\delta}$ fluorinated with ZnF_2 at 400 °C as representative. Figure 6(a) shows ZF-μSR time spectra at several temperatures. There is no evidence of magnetic order in $Sr_2Ir(O, F)_{6-\delta}$ which is contrary to Sr_2IrO_4 and $Sr_3Ir_2O_7$, where one can clearly observe a muon spin precession indicating a long-range magnetic order [27]. However, for $Sr_2Ir(O, F)_{6-\delta}$, each spectrum shows a Gaussian-like slow decay of initial muon spin polarization, which is mainly attributed to randomly oriented nuclear moments. Figures 6(b) and 6(c) show LF-μSR time spectra at 307 and 3.3 K, respectively. Relaxation is completely decoupled (quenched) under a longitudinal field of 100 G at 307 K, indicating that internal field distribution is considerably lower than 100 G. Meanwhile, at a low temperature of 3.3 K, spectra show a decoupling process but still have a slow relaxation even under a field of 1 kG. This suggests that the slow relaxation may be due to a fluctuating local field arising from slowing down of the Ir electronic spins.

These spectra can be reproduced by the product of an exponential relaxation function and a dynamical Gaussian Kubo-Toyabe function (G^{DGKT}) [31]:

$$A(t) = A_0 e^{(-\lambda_e t)} G^{\mathrm{DGKT}}(\Delta_n, \tau_n, H_{\mathrm{LF}}) + A_{\mathrm{BG}}, \qquad (1)$$

where A_0 is the positron decay initial asymmetry (amplitude), λ_e is the muon relaxation rate by electronic spins, Δ_n is proportional to the root-mean square of the local field distribution (Gaussian linewidth) of nuclear magnetic moments, τ_n is the fluctuation correlation time, H_{LF} is the longitudinal field, and A_{BG} is the background asymmetry (=0.0293, mainly from a silver backing plate). Solid lines in Fig. 6 show the result of a least-squares curve-fit. Temperature dependence of respective parameters is shown in Fig. 7.

As shown in Fig. 7(a), λ_e suddenly increases below 250 K, indicating a slowing down of Ir electronic spin fluctuation. This suggests the development of an antiferromagnetic spin correlation between Ir spins, while the magnetic susceptibility

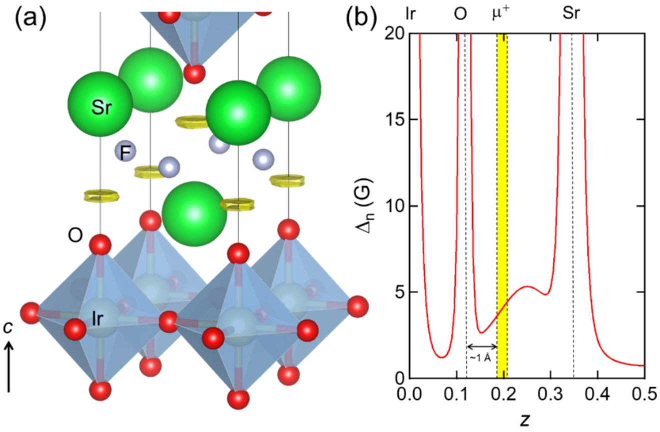

FIG. 8. (a) Schematic illustration of a hypothetical $Sr_2IrO_4F_2$ structure with Hartree potential isosurfaces (yellow lobes). (b) Nuclear-field distribution width Δ_n calculated along z direction. The yellow-shaded area represents Hartree potential minima (see text).

shows no anomaly around 250 K [see Fig. 5(b)]. The magnetic nature of $Sr_2Ir(O, F)_{6-\delta}$ seems essentially the same as the parent compound Sr_2IrO_4 which exhibits a Néel order below 240 K. The absence of magnetic order in $Sr_2Ir(O, F)_{6-\delta}$ may be attributed to antiferromagnetic instability between IrO_2 layers, brought about by elongation of the c axis due to fluorine intercalation. It is known that A_2IrO_4 ($A = $ Sr, Ba) belong to a category of anisotropic Heisenberg spin systems with weak 3D interlayer exchange coupling, possibly rendering them sensitive to changes in interlayer distance [32]. Muon spin relaxation rate λ_e is inversely related to the electronic spin fluctuation rate ν_e on the basis of Redfield's formula [33]:

$$\lambda_e = \frac{2(\gamma_\mu \delta_e)^2}{\nu_e} \; (\nu_e \gg \delta_e), \tag{2}$$

where γ_μ is the muon gyromagnetic ratio ($=2\pi \times 135.54\,\mathrm{MHz/T}$) and δ_e is the average distribution of local magnetic fields ($=100.6\,\mathrm{G}$, which is calculated from $\mu_{\mathrm{eff}} = 0.51\,\mu_{\mathrm{B}}$) at the muon site (0, 0, 0.18), as described later. ν_e is calculated to be ca. 2.4 GHz at 3.3 K, roughly one-tenth in magnitude compared to that of paramagnetic (thermal) spin fluctuation at low temperatures.

Next, we examined the local field related to nuclear magnetic moments. As shown in Figs. 7(b) and 7(c), the Gaussian linewidth Δ_n is narrow ($\sim 0.23\,\mathrm{ms}^{-1}$) and almost constant for all measured temperatures, which are typical characteristics for nuclear moments. The relaxation time τ_n indicates the dynamics of either atom motions (vibrations), or muon motion. If a muon stopping site and Δ_n at a specific point are identified, then we can estimate the fluorine content of our sample, because almost all nuclear moments can be attributed to ^{19}F ($2.6288\,\mu_{\mathrm{N}}$) in $Sr_2Ir(O, F)_{6-\delta}$.

Figure 8(a) shows a hypothetical crystal structure of $Sr_2IrO_4F_2$ with Hartree potential distribution (yellow lobes), calculated by Vienna *Ab initio* Simulation Package (VASP) [34]. A muon might be located between the apical oxygen and Sr, since the Hartree potential exhibits electronegative minima in that region. It is known that a positive muon often forms F-μ^+ or F-μ^+-F bonding states in fluorides with a characteristic muon precession [35]. In our case, these bonding states can be ruled out, since F-μ^+ or F-μ^+-F precessions were not observed [see Fig. 6(a)]. To estimate fluorine content, we compared experimental Δ_n with theoretical Δ_n, obtained by the dipolar-field summation on $Sr_2IrO_4F_2$ [36].

Figure 8(b) shows theoretical Δ_n calculated along z direction from $z = 0$ to 0.5. The above-mentioned potential minima, located in the vicinity of the apical oxygen, are shown in the yellow-shaded area. It is known that positive muon usually stops near O^{2-} ions and forms an O-μ^+ bond of ca. 1 Å [37]. This naturally leads to the assumption that a muon occupies an interstitial position (0, 0, 0.18), which is 1 Å displaced from the apical oxygen [see the double-headed arrow in Fig. 8(b)]. This assumption also implies that fluorine does not occupy apical anion sites. We obtained a theoretical Δ_n of 3.4 G at the position, which is slightly larger than the experimental one (Δ_n of 2.7 G, converts from $\Delta_n = 0.23\,\mu\mathrm{s}^{-1}$). This result suggests that fluorine content is comparatively reduced from the stoichiometric composition of $Sr_2IrO_4F_2$. Based on this analysis, fluorine content is estimated at 1.54. Meanwhile, oxygen content could not be deduced as oxygen has no nuclear moments. Therefore, the chemical composition of ZnF_2-fluorinated product is estimated to be $Sr_2IrO_xF_{1.5}$ with $x = 3.25$, assuming Ir^{4+}. The large fluorine vacancy number can be attributed to a relatively large τ_n in Fig. 7(c). This may also be related to the intercalated fluorine instability in our sample.

IV. CONCLUSION

We have synthesized a new layered iridium oxyfluoride $Sr_2Ir(O, F)_{6-\delta}$ by topochemical fluorination of Sr_2IrO_4 with PVDF, ZnF_2, or CuF_2. The c axis of the products was considerably longer because a fluorine layer had been inserted in between Sr_2IrO_4 rock salt layers. Variations in lattice parameters, dependent on the type of fluorination reagent employed and sintering conditions, suggest that there are differences in fluorine content and/or oxygen vacancies in $Sr_2Ir(O, F)_{6-\delta}$ The carrier transport properties of the fluorinated samples are nonmetallic behavior, which is explained by Efros-Shklovskii VRH mechanism. The canted antiferromagnetism observed in Sr_2IrO_4 was suppressed in $Sr_2Ir(O, F)_{6-\delta}$ regardless of fluorination reagents and conditions. This is probably due to the antiferromagnetic instability between IrO_2 layers resulting from c-axis elongation, in turn caused by fluorine intercalation. We have demonstrated an effective topochemical reaction method for the synthesis of new iridium compounds that have interesting physical properties, similar to those of Sr_2IrO_4. By utilizing this method for other oxides, we anticipate the development of novel compounds with interesting physical properties.

ACKNOWLEDGMENTS

This work was supported by JSPS Grant-in-Aid for Scientific Research on Innovative Areas "Mixed Anion" (Grant No. JP16H6439). The muon experiment at the Materials and Life Science Experimental Facility of the J-PARC was performed under a user program (Proposal No. 2018B0151). This work was partially supported by the KEK-MSL Inter University Research Program. We acknowledge H. Lee for VASP calculations. We also thank Y. Udagawa and Prof. T. Oka at Shibaura Institute of Technology for assistance with EPMA measurements.

[1] B. J. Kim, H. Jin, S. J. Moon, J.-Y. Kim, B.-G. Park, C. S. Leem, J. Yu, T. W. Noh, C. Kim, S.-J. Oh, J.-H. Park, V. Durairaj, G. Cao, and E. Rotenberg, Phys. Rev. Lett. **101**, 076402 (2008).
[2] B. J. Kim, H. Ohsumi, T. Komesu, S. Sakai, T. Morita, H. Takagi, and T. Arima, Science **323**, 1329 (2009).
[3] H. Watanabe, T. Shirakawa, and S. Yunoki, Phys. Rev. Lett. **110**, 027002 (2013).
[4] Z. Y. Meng, Y. B. Kim, and H.-Y. Kee, Phys. Rev. Lett. **113**, 177003 (2014).
[5] X. Chen, T. Hogan, D. Walkup, W. Zhou, M. Pokharel, M. Yao, W. Tian, T. Z. Ward, Y. Zhao, D. Parshall, C. Opeil, J. W. Lynn, V. Madhavan, and S. D. Wilson, Phys. Rev. B **92**, 075125 (2015).
[6] K. Horigane, M. Fujii, H. Okabe, K. Kobayashi, R. Horie, H. Ishii, Y. F. Liao, Y. Kubozono, A. Koda, R. Kadono, and J. Akimitsu, Phys. Rev. B **97**, 064425 (2018).
[7] J. C. Wang, S. Aswartham, F. Ye, J. Terzic, H. Zheng, D. Haskel, S. Chikara, Y. Choi, P. Schlottmann, R. Custelcean, S. J. Yuan, and G. Cao, Phys. Rev. B **92**, 214411 (2015).
[8] C. Zhu, S. Liu, J. Cheng, B. Li, P. Dong, and Z. Wang, EPL **124**, 17004 (2018).
[9] T. F. Qi, O. B. Korneta, S. Chikara, M. Ge, S. Parkin, L. E. De Long, P. Schlottmann, and G. Cao, J. Appl. Phys. **109**, 07D906 (2011).
[10] X. Sun, S. L. Liu, H. Wang, B. Li, J. Cheng, and Z. H. Wang, J. Alloys Compd. **687**, 712 (2016).
[11] Y. K. Kim, O. Krupin, J. D. Denlinger, A. Bostwick, E. Rotenberg, Q. Zhao, J. F. Mitchell, J. W. Allen, and B. J. Kim, Science **345**, 187 (2014).
[12] Y. K. Kim, N. H. Sung, J. D. Denlinger, and B. J. Kim, Nat. Phys. **12**, 37 (2016).
[13] Y. J. Yan, M. Q. Ren, H. C. Xu, B. P. Xie, R. Tao, H. Y. Choi, N. Lee, Y. J. Choi, T. Zhang, and D. L. Feng, Phys. Rev. X **5**, 041018 (2015).
[14] H. Kageyama, K. Hayashi, K. Maeda, J. P. Attfield, Z. Hiroi, J. M. Rondinelli, and K. R. Poeppelmeier, Nat. Commun. **9**, 772 (2018).
[15] L. D. Aikens, R. K. Li, and C. Greaves, Chem. Commun. **21**, 2129 (2000).
[16] P. R. Slater and R. K. B. Gover, J. Mater. Chem. **12**, 291 (2002).
[17] M. Ai-Mamouri, P. P. Edwards, C. Greaves, and M. Slaski, Nature **369**, 382 (1994).
[18] C. Peterson, M. W. Swift, Z. Porter, R. J. Clément, G. Wu, G. H. Ahn, S. J. Moon, B. C. Chakoumakos, J. P. C. Ruff, H. Cao, C. Van de Walle, and S. D. Wilson, Phys. Rev. B **98**, 155128 (2018).
[19] K. M. Kojima, T. Murakami, Y. Takahashi, H. Lee, S. Y. Suzuki, A. Koda, I. Yamauchi, M. Miyazaki, M. Hiraishi, H. Okabe, S. Takeshita, R. Kadono, T. Ito, W. Higemoto, S. Kanda, Y. Fukao, N. Saito, M. Saito, M. Ikeno, T. Uchida, and M. M. Tanaka, J. Phys. Conf. Ser. **551**, 012063 (2014).
[20] See Supplemental Material at http://link.aps.org/supplemental/10.1103/PhysRevMaterials.4.013403 for the atomic coordinates of $Sr_2IrO_4F_2$ generated by a minor structure modification from $Ba_2ZrO_3F_2$.
[21] P. R. Slater and R. K. B. Gover, J. Mater. Chem. **11**, 2035 (2001).
[22] K. Kawahara, A. Chikamatsu, T. Katayama, T. Onozuka, D. Ogawa, K. Morikawa, E. Ikenaga, Y. Hirose, I. Harayama, D. Sekiba, T. Fukumura, and T. Hasegawa, CrystEngComm **19**, 313 (2017).
[23] F. J. Berry, E. Moore, M. Mortimer, X. Ren, R. Heap, P. Slater, and M. F. Thomas, J. Solid State Chem. **181**, 2185 (2008).
[24] A. L. Efros and B. I. Shklovskii, J. Phys. C Solid State Phys. **8**, L49 (1975).
[25] G. Cao, J. Bolivar, S. McCall, J. E. Crow, and R. P. Guertin, Phys. Rev. B **57**, R11039 (1998).
[26] G. Cao, Y. Xin, C. S. Alexander, J. E. Crow, P. Schlottmann, M. K. Crawford, R. L. Harlow, and W. Marshall, Phys. Rev. B **66**, 214412 (2002).
[27] M. Miyazaki, R. Kadono, M. Hiraishi, A. Koda, K. M. Kojima, K. Ohashi, T. Takayama, and H. Takagi, Phys. Rev. B **91**, 155113 (2015).
[28] C. Dhital, T. Hogan, Z. Yamani, C. de la Cruz, X. Chen, S. Khadka, Z. Ren, and S. D. Wilson, Phys. Rev. B **87**, 144405 (2013).
[29] Y. Singh and P. Gegenwart, Phys. Rev. B **82**, 064412 (2010).
[30] Y. Okamoto, M. Nohara, H. Aruga-Katori, and H. Takagi, Phys. Rev. Lett. **99**, 137207 (2007).
[31] P. D. de Reotier and A. Yaouanc, J. Phys. Condens. Matter **4**, 4533 (1992).
[32] H. Okabe, M. Isobe, E. Takayama-Muromachi, A. Koda, S. Takeshita, M. Hiraishi, M. Miyazaki, R. Kadono, Y. Miyake, and J. Akimitsu, Phys. Rev. B **83**, 155118 (2011).
[33] C. P. Slichter, *Principles of Magnetic Resonance*, 3rd ed. (Springer, Berlin, Heidelberg, 1990).
[34] G. Kresse and J. Hafner, Phys. Rev. B **47**, 558 (1993).
[35] J. H. Brewer, S. R. Kreitzman, D. R. Noakes, E. J. Ansaldo, D. R. Harshman, and R. Keitel, Phys. Rev. B **33**, 7813 (1986).
[36] K. M. Kojima, J. Yamanobe, H. Eisaki, S. Uchida, Y. Fudamoto, I. M. Gat, M. I. Larkin, A. Savici, Y. J. Uemura, P. P. Kyriakou, M. T. Rovers, and G. M. Luke, Phys. Rev. B **70**, 094402 (2004).
[37] E. Holzschuh, A. B. Denison, W. Kündig, P. F. Meier, and B. D. Patterson, Phys. Rev. B **27**, 5294 (1983).
[38] K. Momma and F. Izumi, J. Appl. Crystallogr. **44**, 1272 (2011).